ACS APPLIED MATERIALS & INTERFACES

Forum Article

www.acsami.org

Human Fetal Osteoblast Response on Poly(Methyl Methacrylate)/Polystyrene Demixed Thin Film Blends: Surface Chemistry Vs Topography Effects

Raechelle A. D'Sa,*[,†] Jog Raj,[‡] Peter J. Dickinson,[‡] Fiona McCabe,[‡] and Brian J. Meenan[‡]

[†]Centre for Materials and Structures, University of Liverpool, Brownlow Hill, Liverpool L69 3GH, United Kingdom

[‡]Nanotechnology and Integrated Bio-Engineering Centre (NIBEC), University of Ulster, Shore Road, Newtownabbey, BT37 0QB, United Kingdom

Supporting Information

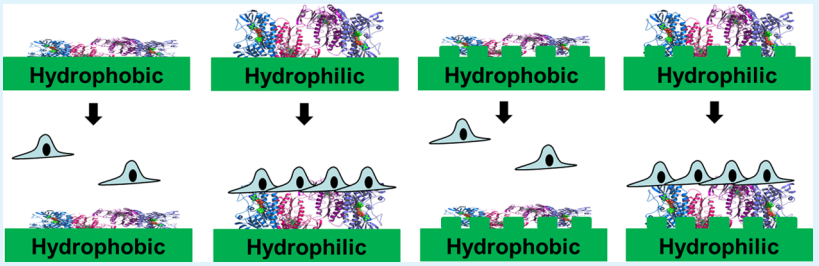

ABSTRACT: Recent advances in materials sciences have allowed for the development and fabrication of biomaterials that are capable of providing requisite cues to instigate cells to respond in a predictable fashion. We have developed a series of poly(methyl methacrylate)/polystyrene (PMMA/PS) polymer demixed thin films with nanotopographies ranging from nanoislands to nanopits to study the response of human fetal osteoblast cells (hFOBs). When PMMA was in excess in the blend composition, a nanoisland topography dominated, whereas a nanopit topography dominated when PS was in excess. PMMA was found to segregate to the top of the nanoisland morphology with PS preferring the substrate interface. To further ascertain the effects of surface chemistry vs topography, we plasma treated the polymer demixed films using an atmospheric pressure dielectric barrier discharge reactor to alter the surface chemistry. Our results have shown that hFOBs did not have an increased short-term cellular response on pristine polymer demixed surfaces. However, increasing the hydrophilicty/wettability of the surfaces by oxygen functionalization causes an increase in the cellular response. These results indicate that topography alone is not sufficient to induce a positive cellular response, but the underlying surface chemistry is also important in regulating cell function.

KEYWORDS: *surface topography, surface chemistry, polymer demixing, cellular response, human fetal osteoblasts, plasma surface modification*

1. INTRODUCTION

One of the main goals in the field of biomaterials and tissue engineering is to identify and utilize nonbiological cues to control cellular response. This control of cellular response includes aspects such as cell adhesion, migration, proliferation, cell-to-cell communication, and expression of a desired phenotype. The ability to predictably control cellular response will have immense implications for tissue engineering with benefits ranging from increased biocompatibility to directing stem cells. Currently, many material science approaches to control cellular response are showing significant promise, however, there is still a lack of fundamental understanding on how these nonbiological cues influence cell−biomaterial interactions. These cues include surface properties such as chemistry, topography, charge, interfacial free energy, wettability, stiffness, etc.[1,2]

The ability to control the response of cells using variations in substratum topography is a heavily researched strategy as these biomimetic cues resemble the nanoscale pores, protrusions, pits, fibers, and particles that make up the extracellular matrix.[2−6] Although it has been shown that cells may behave alike to similar topographies on chemically different surfaces,[7] a "pure" topographical cue needs to be examined using the same surface chemistry. This is because there could be a difference in the protein adsorption behavior on the surface chemistries, which adds an extra variable to the equation. Theoretically, surface chemistry and topography can be varied independently, however it is very difficult to do in practice. Indeed, very few studies have endeavored to differentiate between chemical and topographical cues. In this paper, we attempt to correlate

Special Issue: Current Trends in Functional Surfaces and Interfaces for Biomedical Applications

Received: August 29, 2015
Accepted: December 4, 2015

DOI: 10.1021/acsami.5b08073
ACS Appl. Mater. Interfaces XXXX, XXX, XXX−XXX

cellular behavior to either surface chemistry or topographical influences.

Polymer demixing is an economical fabrication methodology for developing nanotopographies compared with precise, but more expensive techniques such as electron beam lithography. This technique entails the phase separation of polymer blends which spontaneously occurs upon spin coating.[8] Recently, this technique has been widely used to investigate the nanotopographical effects of islands of various heights on cellular response.[9−16] Dalby and co-workers have shown endothelial cells and fibroblasts had a greater cellular response to the 13 nm nanoisland-laden surface in comparison to the other topographies.[16] Donahue and co-workers have investigated fetal osteoblastic cell response to randomly distributed nanoisland topography with varying heights (11, 38, and 85 nm) produced by PS/polybromostyrene (PBrS)[11] and poly(lactic acid)/PS.[10] Cells displayed island-conforming lamellipodia spreading, and filopodia projections which appeared to play a role in sensing the nanotopography. Cells cultured on 11 nm high islands displayed significantly enhanced cell spreading and larger cell dimensions than cells on larger nanoislands or flat controls.[10,11] We have recently demonstrated the human mesenchymal stem cells responded to the poly(methyl methacrylate)/polycaprolactone (PMMA/PCL) demixed nanotopographies in terms of cell adhesion and possibly differentiation.[15]

Poly(methyl methacrylate) (PMMA)/ Polystyrene (PS) is a well-known immiscible polymer blend that has been studied by the polymer demixing process previously.[17−24] Ton-That et al. have previously shown that PMMA/PS demixed films in chloroform form nanoislands and nanopits depending on the ratio of each polymer.[19] Nanoislands were observed when the PMMA mole fraction was greater than 0.5 with PMMA segregating to the air interface.[19] We have chosen this polymer blend as our group has significant experience in studying the effects of surface modification of PMMA and PS by atmospheric pressure plasma treatment using a dielectric barrier discharge (DBD) to increase in cellular response.[25−28] In this paper, we use this polymer blend system to generate nanotopographies with one polymer segregating to the surface, thereby analyzing cellular response with differing topographies under the same surface chemistry. These polymer blends were also plasma treated to see whether altering the surface chemistry while maintaining a similar topography will have an effect on the cellular behavior. X-ray photoelectron spectroscopy (XPS) and time-of-flight secondary ion mass spectrometry (ToF-SIMS) have been used to determine the surface chemistry of the blends. Atomic force microscopy has been used to characterize the topographical features obtained by polymer demixing process and subsequent plasma treatment. The short-term cellular response of these surfaces was examined using human fetal osteoblasts (hFOBs) in terms of cell viability and morphology. hFOBs were used in this study to develop a fundamental understanding of how osteoblasts behave to chemical and topographical controls, which will pave the way to designing surfaces that can direct the behavior of mesenchymal stem cells.

2. MATERIALS AND METHODS

2.1. Spin-Coating of PMMA/PS Blend Films. Glass coverslips (13 mm diameter) were cleaned by immersing them in 25% ammonia: 30% hydrogen peroxide in a 1:9 ratio for 10 min. The coverslips were subsequently rinsed in Milli-Q water, dried and immersed in a 5% solution of chlorotrimethylsilane (CTMS) in *n*-hexane to render the surfaces hydrophobic. The coverslips were than washed thoroughly with *n*-hexane and toluene and left to air-dry before spin coating. PS (MW = 280 000 Da) and PMMA (MW = 350 000 Da) were used as obtained (Sigma-Aldrich, UK). A series of polymer solutions were prepared at 75:25 ($PMMA_{75}PS_{25}$), 50:50 ($PMMA_{50}PS_{50}$) and 25:75 ($PMMA_{25}PS_{75}$) w/w ratios and then dissolved in chloroform to have a total polymer concentration of 1% w/w. Aliquots of the solutions were spin coated onto freshly cleaned glass coverslips and rotated at 4000 rpm for 2 min using a Pi-Kem SCS G3P-12 Spin coater. Spin-coated films were dried at room temperature with no annealing.

2.2. Atmospheric Plasma Treatment. Plasma surface treatment was carried out at atmospheric pressure via exposure to a highly controlled dielectric barrier discharge (DBD) regime. The operational characteristics of the DBD reactor (Arcotec GmbH, Mönsheim, Germany) have been described in detail elsewhere.[25,29] Briefly, the coverslips were placed on a moving platen that is the ground electrode and passes under three metal wire working electrodes giving rise to a microstreamer type electrical discharge condition. The samples are treated with a certain calculated energy dose conditions corresponding to a range of different power densities (Pd) and residence times in the plasma. All DBD treatment of polymer demixed samples was carried out at a platen transit speed through the plasma region of 0.48 m/s and at a plasma dose of 1.04 J/cm^2.

2.3. Contact Angle Analysis. Static contact angle (CAM 2000, KSV Instrument Ltd.; Finland) was used to determine changes in the surface wettability for all samples. Measurements were made 48 h post treatment to allow for any relaxation of the surface to occur. A 5 μL drop of distilled water was dropped onto the surface and the static contact angle was measured at 0 and 5 min. At least five readings were performed per sample type and the corresponding average values and standard deviations were recorded.

2.4. X-ray Photoelectron Spectrometry Analysis. X-ray photoelectron spectroscopy (XPS) was carried out using a Kratos Axis Ultra DLD spectrometer (Kratos, Manchester, UK) using a monochromated AlKα X-ray (1486.6 eV) source operating at a power of 150 W (voltage: 15 kV, current: 10 mA). All spectra were recorded at a pressure of $<5 \times 10^{-8}$ Torr using a "slot" aperture. Any charging effects were neutralized using a magnetic immersion lens. Spectra were calibrated by setting the C−C/C-H component of the high resolution C 1s spectra to 285.0 eV. Wide energy survey scans and high resolution scans were recorded at a pass energy of 160 and 20 eV, respectively. Three separate areas on each sample were recorded and the average results are reported as atomic % concentrations (at. %) ± standard deviation. Spectra were processed using CasaXPS version 2.3.12 software (Casa software, UK) after subtraction of a linear background and determination of areas for the most intense spectral lines for all the elements detected. Spectra were curve fitted after linear background subtraction using a mixed Gaussian−Lorentzian (70:30) function. The full width half-maximum values have been maintained under 2 eV. The electron attenuation length of the C 1s photoelectron in a polymeric matrix can be assumed to be ∼3 nm.[30] This corresponds to an approximate value for the sampling depth of 5−10 nm when the emission angle is normal to the surface.[31] Therefore, 95% of the detected signal originates from this sampling region.

2.5. Time-of-Flight Secondary Ion Mass Spectrometry Analysis. Time-of-flight secondary ion mass spectrometry (ToF-SIMS) was carried out using a ToF-SIMS V (ION-TOF GmbH, Germany) instrument. The primary ion source was a bismuth liquid metal ion gun (LMIG) which generated Bi3++ cluster ions operated in conjunction with a reflectron analyzer and microchannel plate detectors with a post acceleration of 20 kV. A flood gun was used in a pulsed mode to neutralize any charging effects. Analysis was maintained at a static SIMS limit (i.e., < 1012 cm^{-2}) via the primary ion dose density. IonSpec Version 4.1.0.1 (ION-TOF GmbH, Germany) were used for spectral acquisition on spot size of 100 μm × 100 μm at a resolution of 512 × 512 pixels in the high current bunched mode (mass resolution: $m/\Delta m$: 8000). Spectra were calibrated using known hydrocarbon masses in the positive ion mode.

2.6. Atomic Force Microscopy Analysis. AFM analysis was carried out using a Digital Instruments (DI) NanoScope SPM (Vecco

DOI: 10.1021/acsami.5b08073
ACS Appl. Mater. Interfaces XXXX, XXX, XXX−XXX

Metrology Group, USA) instrument in tapping mode using a silicon tip and a cantilever with a spring constant of 40 N m^{-1}, operating at a resonant frequency of 300 kHz and scan rate 1 Hz. Samples were analyzed over a 10 μm × 10 μm area at a resolution of 512 × 512 pixels. Image processing and interpretation was carried out using the NanoSope 6.11r1 software (Vecco Average R_a (mean roughness) and R_q (root-mean-square roughness) were calculated from at least three replicates including the center and edge regions of the samples.

2.7. hFOB Cell Culture. hFOB (1.19, ATCC number CRL-11372) cells were subcultured in DMEM-Ham's F-12 1:1 media (GIBCO) supplemented with 10% fetal bovine serum (FBS, Hyclone) and 1% penicillin−streptomycin on tissue culture polystyrene (TCPS) and incubated at 37 °C under an atmosphere of 5% CO_2. Before, culturing on the polymer demixed samples, cells were rinsed in phosphate-buffered saline (PBS) and incubated with trypsin-EDTA solution to remove the cells from TCPS. The cells were then seeded on the substrates at a density of 30,000 cells/cm^2 and allowed to adhere on each test substrate and rinsed with PBS and the remaining adherent cells were subjected to assays at the desired time points.

For cell culture studies, the test substrates were sterilized by exposure to UV light for 1 h. A stock solution of 0.6% Agar (Sigma-Aldrich, UK) in Milli-Q water was freshly prepared and autoclaved at 123 °C for 15 min. 200 μL of the hot Agar was pipetted into sterile six-well plates with subsequent careful placement of the test substrates. The agar was used as gelling agent sticking test substrates to the six-well to prevent adhesion of cells to the underside of the substrates.

2.8. MTT Cell Viability Assay. hFOBs were cultured on each test substrate and assayed using the MTT cell viability assay at 24 and 72 h post seeding. A stock solution of 5 mg/cm^3 of [3-(4,5-dimethylthiazol-2-yl)-2,5-diphenyltetrazolium bromide] (MTT, Sigma-Aldrich, UK) was prepared, filtered (0.2 mm filter) and stored at 4 °C. At the requisite time points, the media was aspirated and replaced with 2 cm^3 of phenol-free DMEM media (Gibco, UK) with an MTT solution of 500 μg/cm^3. The surfaces were then incubated at 37 °C and 5% CO_2 until the purple formazan product was visible (~2 h). NAD(P)H-dependent cellular oxidoreductase enzymes are capable of reducing the tetrazolium dye MTT 3-(4,5-dimethylthiazol-2-yl)-2,5-diphenyltetrazolium bromide only in viable cells to its insoluble formazan, which has a purple color. The media was then aspirated and cells were subsequently solubilized with 350 μL of 0.1 M HCl in propanol to each well and plates were placed on a gyro-rocker for 10 min. Aliquots (100 μL) from each well were placed in a 96-well plate giving a 9 replicates of each sample. A Tecan SunriseTM (TECAN GmbH, Austria) microplate reader fitted with a 570 nm filter was used to measure the absorbance (optical density).

2.9. Cell Staining and Morphology. Cell staining was performed 48h post seeding by rinsing the cells (3 × 5 min) with copious amounts of ice-cold PBS. The cells were then subsequently fixed in 3.7% PFA/PBS and solubilized in 0.1% Triton X-100/PBS at 4 °C for 20 min. PFA was removed by washing the cells with PBS (3 × 5 min) and blocked with PBS containing 1.0% BSA, 5% normal goat serum (NGS) for 60 min followed by washing with PBS (3 x5 min). Cytoskeletal actin was visualized by incubating the samples phalloidin Alexa Fluor 488 (Molecular Probes, UK) at a concentration of 25 U/cm^3. The samples were rinsed in PBS (3 × 5 min) and mounted with Vectashield Mounting Medium containing 1.5 μg/cm^3 of DAPI (4′-6-diamidino-2-phenylindole) counterstain (Vector Laboratories, UK) which was used to visualize the nuclei. The slides were sealed with a clear varnish and analyzed using an epifluorescence microscope (Nikon Eclipse 80*i*).

2.10. Statistical Analysis. One way analysis of variance (ANOVA) statistical analysis was carried out using Origin (v. 7.0383, OriginLab Corporation, USA) to determine equivalence of variance between pairs of samples. A Bonferroni multiple comparison test was used to determine significance with a value of $p < 0.05$ was taken as being statistically significant. Results are reported as means ± standard deviation.

3. RESULTS

3.1. Wettability: Contact angle. Static contact angles were measured for all three of the demixed polymer surfaces before and after DBD treatment and are given in Figure 1. The individual polymers studied were both hydrophobic in nature with contact angles of 84 and 95° for PMMA and PS, respectively. After blending the two polymers, the contact angle for the $PMMA_{75}PS_{25}$, $PMMA_{50}PS_{50}$ and $PMMA_{25}PS_{75}$ films are 87, 73, and 88°, respectively when the measurement is taken immediately. After 5 min the contact angle drops by at least 5° for each demixed film as seen in Figure 1. This phenomenon does not occur on flat substrates (data not shown) and is indicative of a topography induced wettability change observed in contact angle measurement. Topography is hypothesized to enhance the wettability of a substrate by increasing the surface area.[32] As such, the contact angle of nanotextured surfaces is lower than their flat counterparts as the surface roughness is impregnated with the water droplet.[33] After DBD treatment, there is a decrease in contact angle for all 3 of the demixed surfaces studied. The contact angle for the $PMMA_{75}PS_{25DBD}$, $PMMA_{50}PS_{50DBD}$ and $PMMA_{25}PS_{75DBD}$ films are 61, 69 and 79°, respectively. Once again, a topography induced wettability change is observed with the contact angle measurement after 5 min.

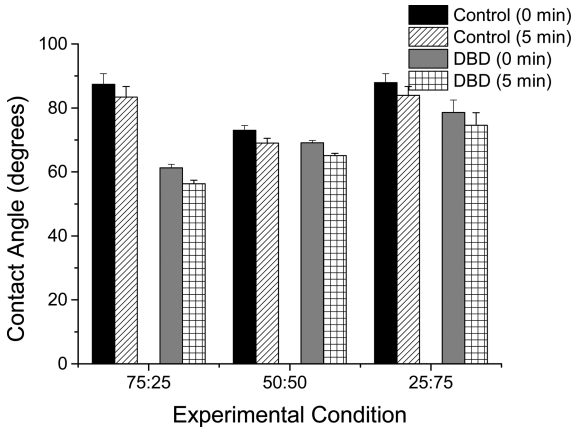

Figure 1. Static water contact angle measurements taken at time 0 and after 5 min for the various polymer demixed surfaces. The ratios given in the *x*-axis represent a ratio of PMMA:PS.

3.2. Surface Chemistry of Polymer Demixed Films: XPS and ToF-SIMS Analysis. *3.2.1. XPS Analysis.* The surface chemistry of the polymer demixed films pre- and post-DBD treatment were analyzed using XPS. The high-resolution C 1s spectra are presented in Figure 2 and the elemental at. % with the associated C1 curve fitted values are given in Tables S1 and S2. Pure PMMA contains both C and O and can be curve fitted into four components with binding energies at 285.0 eV (C−C/C−H), 285.8 eV (C−C(C═O)—O), 286.9 eV (C−O), and 289.4 eV (O═C−O). Pure PS does not contain oxygen in its backbone and C 1s peak can be peak fitted into the aromatic and aliphatic C−C/C−H component at 285.9 eV and the $\pi-\pi^*$ shakeup component at 292.0 eV. This aromatic and aliphatic C−C/C−H distinction can be made only for pure PS. Similarly to the previous reported studies there is a higher contribution from PMMA components (C−O, O−C═O) when there is an increase in PMMA in the blend composition as seen in Figure 2c, e, g. To analyze which polymer segregates

DOI: 10.1021/acsami.5b08073
ACS Appl. Mater. Interfaces XXXX, XXX, XXX−XXX

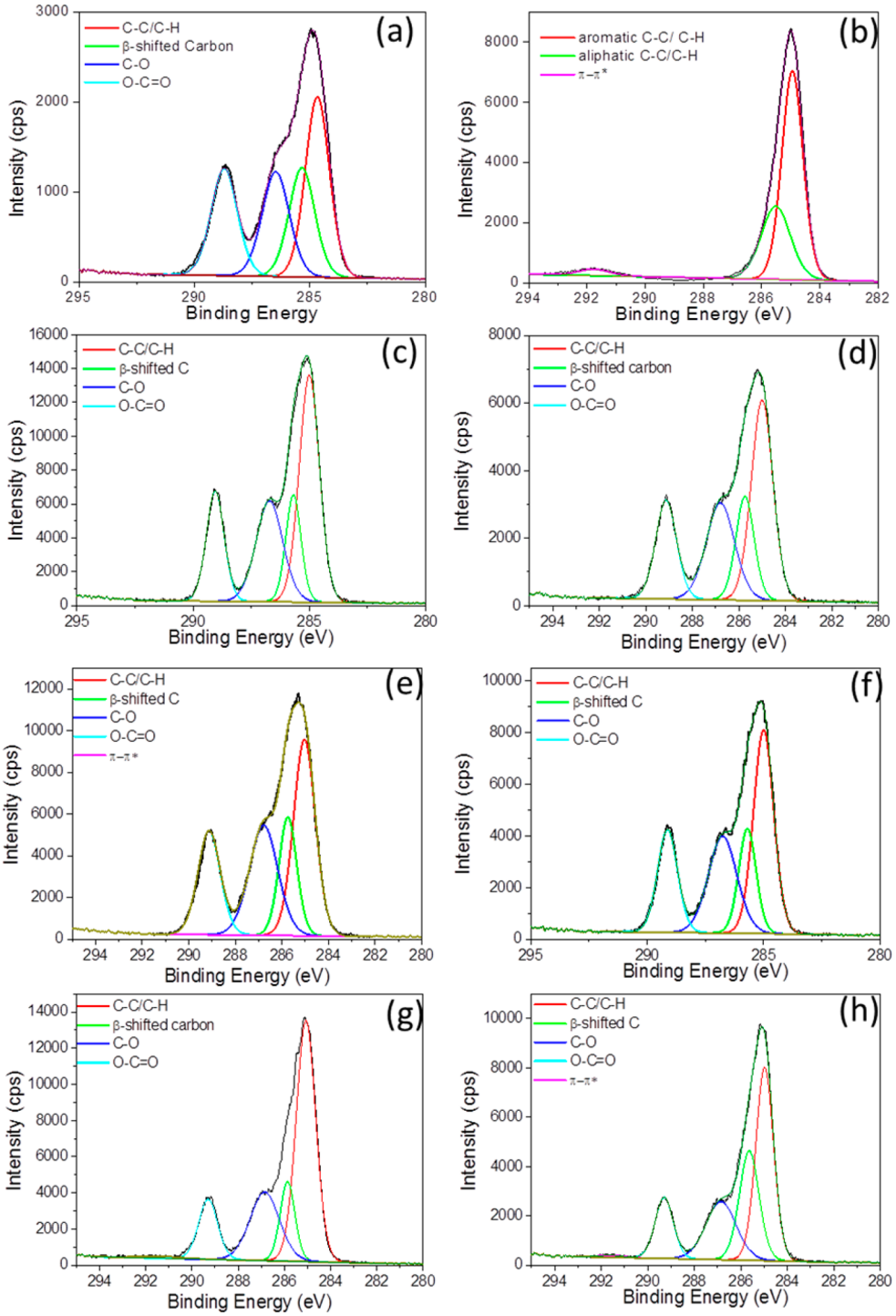

Figure 2. High-resolution C 1s spectra of (a) PMMA, (b) PS, (c) $PMMA_{75}PS_{25}$, (d) $PMMA_{75}PS_{25DBD}$, (e) $PMMA_{50}PS_{50}$, (f) $PMMA_{50}PS_{50DBD}$, (g) $PMMA_{25}PS_{75}$, and (h) $PMMA_{25}PS_{75DBD}$.

to the air interface, we calculated the surface composition of the blend films by evaluating the O 1s peak as this was attributed solely to PMMA in a similar approach to that reported by Ton-That et al.[19] Briefly, the surface fraction of PMMA was calculated by comparing the ratio of the PMMA component (O 1s peak) to that of a pure PMMA standard. As such the O/C ratio is given in eq 1

$$\left(\frac{O}{C}\right)_{exp} = \frac{XO_{PMMA}}{XC_{PMMA} + (1 - X)C_{PS}} \quad (1)$$

Where X is the molar PMMA surface concentration in the demixed film; O_{PMMA} and C_{PMMA} and C_{PS} are the at % of oxygen and carbon concentration in the pure films of PMMA and PS, respectively. Using eq 1, the surface PMMA fraction was calculated as a function of the PMMA bulk molar concentration and the results are presented in Figure 3. All of the demixed films are located above the equivalent composition line indicating that the molar fraction of PMMA is greater in the surface than in than in the bulk indicating that

DOI: 10.1021/acsami.5b08073
ACS Appl. Mater. Interfaces XXXX, XXX, XXX−XXX

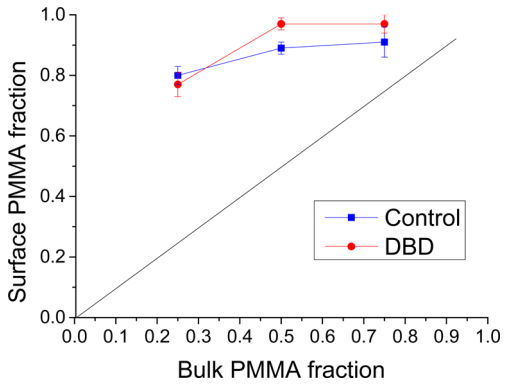

Figure 3. Plot of film surface PMMA fraction vs bulk PMMA fraction in the demixed films. Data obtained using high resolution C 1s- and O 1s-based XPS measurements and eq 1. Linear line is an equivalent composition line.

PMMA segregates to the air interface while PS segregates to the substrate interface.

3.2.2. ToF-SIMS. Positive-ion ToF-SIMS spectra of the three polymer blends before and after DBD treatment are presented in Figure 4. The main peaks detected are at m/z 15 (CH_3^+), 59 ($C_2H_3O_2^+$), 69 ($C_4H_5O^+$), corresponding to PMMA and m/z 77 ($C_6H_5^+$) and 91 ($C_7H_7^+$) corresponding to polystyrene. The characteristic peaks are consistent with those for PMMA and PS reported previously.[29] In all the spectra, the characteristic PS peaks were lower intensity than the PMMA peaks which might indicate that PS segregates to the substrate as ToF-SIMS is a very surface sensitive technique and analyzes only the top 2 nm of the surface. In order to calculate which polymer segregates to the air interface, ToF-SIMS peaks that were characteristic to either PMMA or PS exclusively were used. For PMMA, m/z 15, 59, and 69 were the fragments used and for PS, m/z 77 and 91

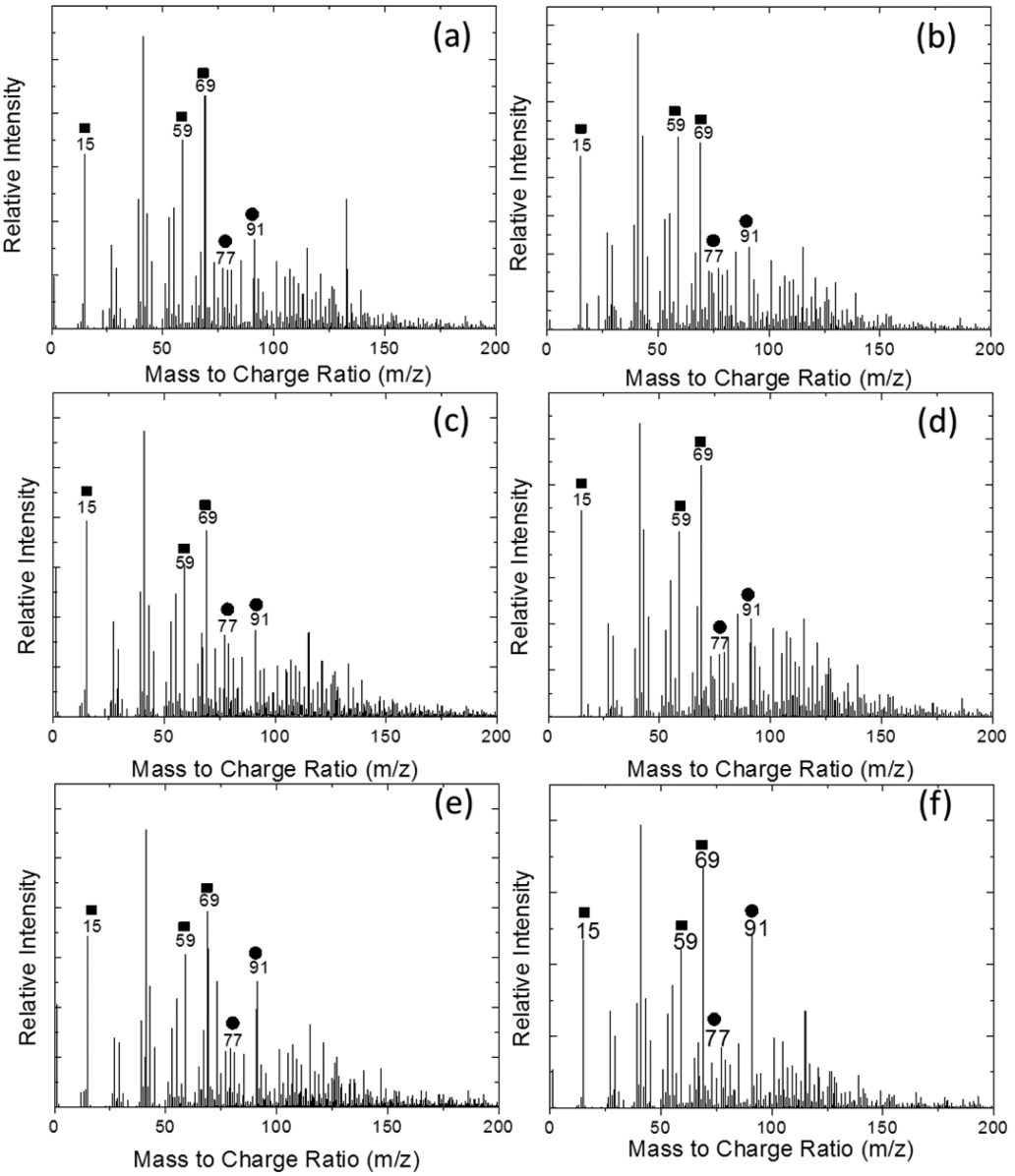

Figure 4. Positive ion ToF-SIMS spectra for (a) $PMMA_{75}PS_{25}$, (b) $PMMA_{75}PS_{25DBD}$, (c) $PMMA_{50}PS_{50}$, (d) $PMMA_{50}PS_{50DBD}$, (e) $PMMA_{25}PS_{75}$, (f) $PMMA_{25}PS_{75DBD}$. The y-axis represents relative intensity and units are not displayed as they are different maximum intensities. ■ Peaks are characteristic for PMMA and ● peaks are characteristic for PS.

DOI: 10.1021/acsami.5b08073
ACS Appl. Mater. Interfaces XXXX, XXX, XXX−XXX

were used. The surface composition of PMMA in the spin-coated film surface was calculated as per eq 2:

$$X_{\mathrm{SIMS}}=(I_{f15}+I_{f59}+I_{f69})/(I_{f15}+I_{f59}+I_{f69})+(I_{f77}+I_{f99}) \quad (2)$$

Where X molar PMMA surface concentration in the demixed film; I_{f15}, I_{f59}, I_{f69}, I_{f77} and I_{f91} are the normalized intensities of the fragments. Using eq 2, the surface PMMA fraction was calculated as a function of the PMMA bulk molar concentration and the results are presented in Figure 5. All of the demixed

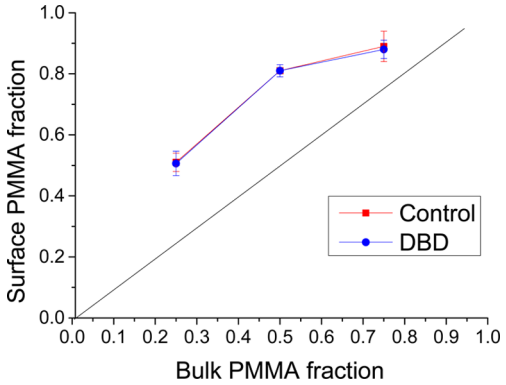

Figure 5. Plot of film surface PMMA fraction vs bulk PMMA fraction in the demixed films. Data obtained using positive ion ToF-SIMS intensities and equation (s). Linear line is an equivalent composition line.

films are located above the equivalent composition line, this shows that the surface concentration of PMMA is greater than in the bulk, indicating that PMMA segregates to the air interface while PS segregates to the substrate interface.

3.2.3. Surface Chemistry of PMMA/PS Demixed Films. From Figures 3 and 5, the XPS and SIMS data clearly shows that all three demixed films and their plasma treated counterparts are situated above the equivalent composition line. Therefore, the concentration of PMMA is greater in the surface than in the bulk indicating that PMMA has segregated to the air interface and PS has segregated to the substrate interface. A salient point of note is that the sampling depths of the two techniques are different; ToF-SIMS has a sampling depth of 2 nm while XPS has a sampling depth of 5−10 nm. Furthermore, these sampling depths are approximate values and are not defined in the same way as the relative ToF-SIMS intensities are assumed to be equal for the calculations, but in reality are not necessarily so. Moreover the lateral area of analysis for the two techniques is also different; we have set the ToF-SIMS to have an area of analysis of 100 μm^2, while XPS has a spot size of 700 × 300 μm^2. From Figure 3, the XPS spectra clearly show a dominance of PMMA at the air interface regardless of whether the samples were DBD treated. ToF-SIMS spectra also displayed an increase in PMMA signal compared to the PS signal at an air interface (Figure 4), and even a large disparity in sensitivities would not alter the dominance of the PMMA segments at the film surface. Therefore, as ToF-SIMS is much more surface sensitive, these results indicated that PMMA segregates to the air interface. However, as the PS peaks do not disappear completely, this would indicate that perhaps at certain points the PMMA overlayer is very thin or nonexistent to allow for PS to be visible by ToF-SIMS analysis.

3.3. Surface Topography: AFM. AFM was used to analyze the topography of the various surfaces. The pure polymer films, exhibit flat surfaces with few surface features (Figure S1 in the Supporting Information). The Rq and Ra roughness for the pure and demixed films are given in Table 1. The topography of the polymer demixed films varied depending on the ratios of the polymers and are given in Figure 6 (shown at different maximum heights). When PMMA was in excess the films took on a nanoisland topography with an average peak height of 27.7 nm (Figure 6a, Table 1). After DBD treatment, some etching of the nanoislands had occurred, however, the randomly distributed nanoisland topography is still present, with the height of the features reducing to 19.2 nm (Figure 6d, Table 1). The increase in the nanoisland topography with an increase in the PMMA bulk concentration points to the nanoislands being most likely being a PMMA rich phase. When PS is in excess, a nanopit topography dominates with a pit depth of 14.9 nm for the $PMMA_{25}PS_{75}$ surface. DBD treatment causes etching of the demixed film by increasing the depth of the pits to 27.2 nm (Figure 6f, Table 1). The $PMMA_{50}PS_{50}$ surface has a topography of interconnected islands and pits with a feature height of 54.1 nm (Figure 6b, Table 1). The $PMMA_{50}PS_{50DBD}$ surface has nanoislands with a feature height of 57.5 nm (Figure 6e, Table 1).

Statistical analysis was undertaken to determine whether the peak-to-peak differences, height/depth and roughness values for the various surfaces of interest changed significantly after DBD treatment with the resulting data given in Table 1. The only surface found to have a statistical significant change in peak to peak distance after DBD treatment was $PMMA_{25}PS_{75}$. In addition, the height/depth values for both the $PMMA_{75}PS_{25}$ and $PMMA_{25}PS_{75}$ surfaces were statistically different after exposure to plasma processing. Although statistical significance was seen in these cases, it is of note that type of feature does not change, that is, the nanoisland/nanopit topography remains consistent. Furthermore, these feature heights remain under 70 nm. Nanoisland heights of <70 nm are reported to increase

Table 1. Topography of PMMA/PS Demixed Thin Films

sample	topography	peak to peak (μm)	feature height/depth (nm)	R_q (nm)	R_a (nm)
PMMA	flat			0.9 ± 0.1	0.7 ± 0.0
PS	flat			1.2 ± 0.2	1.0 ± 0.1
$PMMA_{75}PS_{25}$	islands	0.5 ± 0.1	27.7 ± 4.4[a]	9.3 ± 1.1[a]	7.5 ± 0.8[a]
$PMMA_{50}PS_{50}$	islands/pits	2.4 ± 0.4	54.1 ± 13.2	31.6 ± 9.8	27.2 ± 0.3
$PMMA_{25}PS_{75}$	pits	0.6 ± 0.1[a]	14.9 ± 5.5[a]	5.5 ± 0.8[a]	4.0 ± 0.6[a]
$PMMA_{75}PS_{25DBD}$	islands	0.6 ± 0.2	19.2 ± 5.2[a]	6.4 ± 0.5[a]	5.1 ± 0.4[a]
$PMMA_{50}PS_{50DBD}$	islands/pits	2.3 ± 0.6	57.5 ± 18.2	23.0 ± 1.5	19.1 ± 1.4
$PMMA_{25}PS_{75DBD}$	pits	1.1 ± 0.2[a]	27.2 ± 9.0[a]	8.7 ± 0.2[a]	6.8 ± 0.2[a]

[a]Indicates statistical significance ($p < 0.05$) between the control and DBD-treated surfaces.

DOI: 10.1021/acsami.5b08073
ACS Appl. Mater. Interfaces XXXX, XXX, XXX−XXX

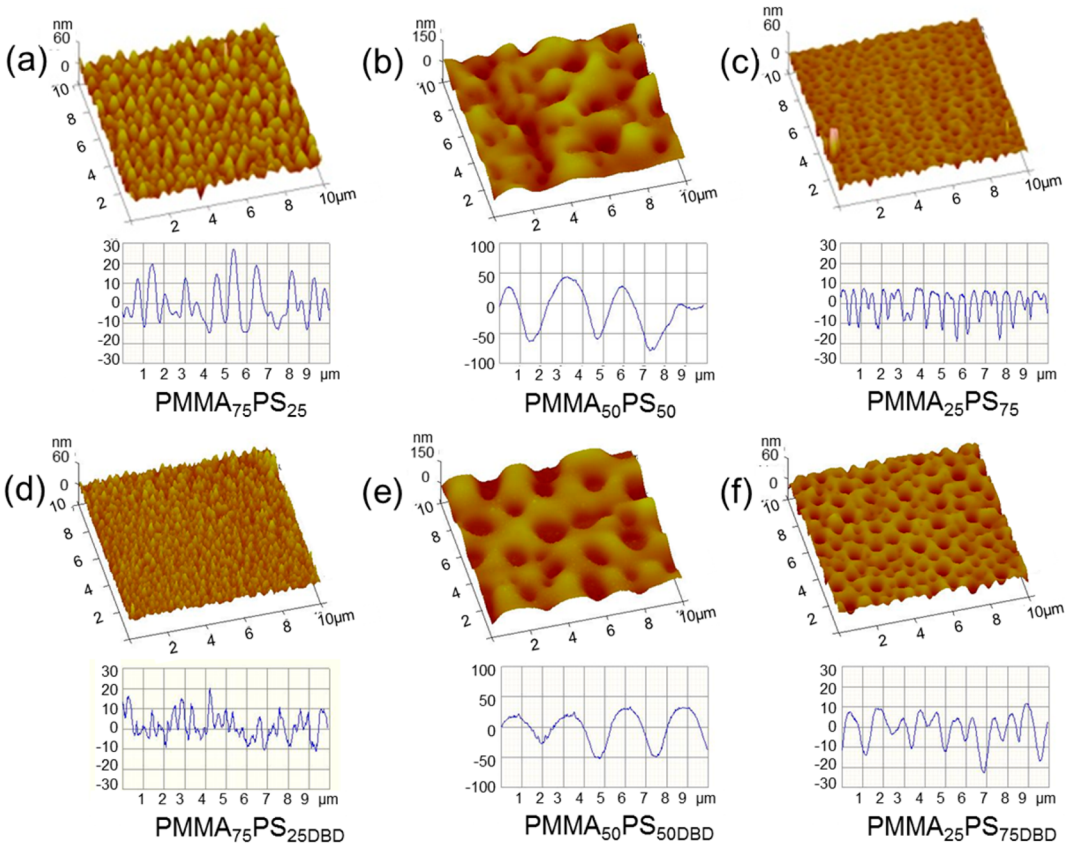

Figure 6. AFM height mode images of PMMA/PS demixed thin films. 10 ×10 μm^2 size images are shown at different *z*-axis maximum heights. (a, c, d, f) Maximum *z*-height of 60 nm and (b, e) maximum height of 150 nm.

cellular adhesion as feature above this threshold disrupt integrin clustering and thereby cell adhesion.[4] Indeed hFOBs grown on 11 nm high islands displayed significantly enhanced cell spreading and larger cell dimensions than cells on larger nanoislands (38 and 85 nm) or flat controls.[10,11] Integrin clustering and focal adhesion reinforcement is unaffected on nanopits with a diameter of <70 nm irrespective of pit depth. Furthermore, increasing the interfeature spacing to the submicron scale facilitates cell-basal substratum interactions below a feature height of ~70 nm.[4] Therefore, although there is some etching of the polymer after DBD treatment, the nanotopographies remain in the range that have been previously shown to increase cellular response.[4] All of the blend films display a large surface excess of PMMA, which indicates that these surfaces are not at thermodynamic equilibrium since the surface energy of PS is lower than that of PMMA.[17,19,34] Figure S1 along with our previously reported findings[25] indicates that DBD treatment of pure PMMA results in oxygen functionalization and etching of the polymer while PS results in mainly oxygen functionalization. As etching of the nanoislands and pits is observed post DBD treatment of the demixed films here, this provides more corroborating evidence to PMMA occupying the air interface.

3.4. Biological Analysis. *3.4.1. MTT Cell Viability.* Short-term cellular response was analyzed using an MTT cell viability assay. Figure 7 shows the viability of the hFOBs on the various surfaces 24 and 72 h post seeding. hFOB cell viability was statistically significantly lower on all the control polymer demixed surfaces ($PMMA_{75}PS_{25}$, $PMMA_{50}PS_{50}$, and $PMMA_{25}PS_{75}$) when compared with the DBD treated

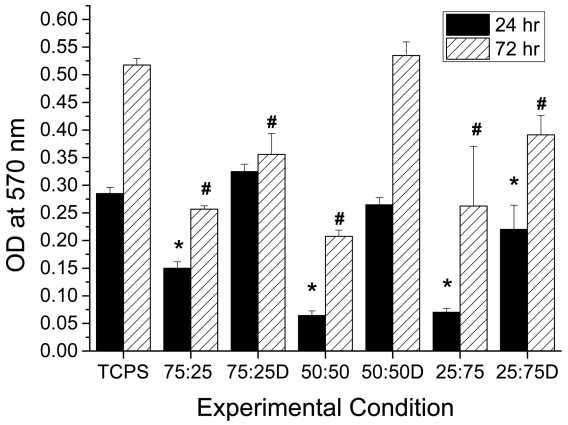

Figure 7. MTT viability assay data for hFOBs 24 and 72 h in culture on the various demixed surfaces. The ratio given on the *x*-axis represents PMMA:PS. *Statistical significance at $p < 0.05$ for 24 h compared with TCPS, # $p < 0.05$ for 72 h compared with TCPS.

($PMMA_{75}PS_{25DBD}$ and $PMMA_{25}PS_{75DBD}$). All 6 polymer demixed surfaces did not respond as well as cells cultured on tissue culture polystyrene (TCPS) which was used as the positive control. The only surface that was comparable to TCPS was the $PMMA_{50}PS_{50DBD}$ surface, which showed no difference in the number of viable cells 24 and 72 h after seeding when compared with TCPS.

The response of hFOB cells to pristine and DBD plasma treated PMMA and PS surfaces are given in Figures S2 and S3, respectively. From these experiments, it can clearly be seen that there is a statistically significant increase in the number of viable

DOI: 10.1021/acsami.5b08073
ACS Appl. Mater. Interfaces XXXX, XXX, XXX−XXX

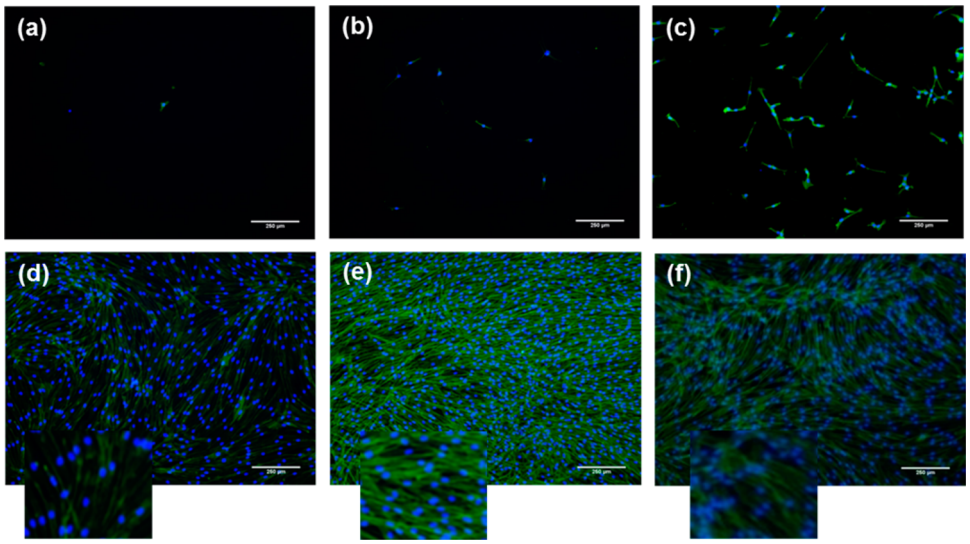

Figure 8. Fluorescent images of hFOBs dual stained for actin (green) and nuclei (blue) after 48 h in culture showing the cytoskeleton in cells on (a) $PMMA_{75}PS_{25}$, (b) $PMMA_{50}PS_{50}$, (c) $PMMA_{25}PS_{75}$, (d) $PMMA_{75}PS_{25DBD}$, (e) $PMMA_{50}PS_{50DBD}$, and (f) $PMMA_{25}PS_{75DBD}$. Insets in d–f are enlargements of the figures. The scale bar represents 250 μm.

cells on the plasma treated PMMA and PS surfaces compared to the pristine pure flat equivalents. These results corroborate our previously published work which has shown that lens epithelial cells do not adhere and proliferate well on hydrophobic flat PMMA and PS but do so effectively on the corresponding DBD treated surfaces.[25] Therefore, these results suggest that for certain types of cells, topography alone is not sufficient to instigate a positive response, but rather a change in surface chemistry, in this case, increased oxygen functionality leading to increased hydrophilicity, provides the requisite cues for enhancing cellular response. In the case of the polymer demixed systems investigated here, it is found that a change in topography is not sufficient to instigate increased cell adhesion and proliferation of hFOBs. These results demonstrate that it is necessary to consider the full physicochemical composition of a biomaterial surface in the context of controlling cell response thereon.

3.4.2. hFOB Morphology. The morphology of hFOB cells on the various surfaces was studied by microscopic analysis of the cytoskeleton and nuclei of fluorescently labeled cells 48h postseeding. The untreated polymer demixed surfaces ($PMMA_{75}PS_{25}$, $PMMA_{50}PS_{50}$, and $PMMA_{25}PS_{75}$) showed only a few spindle shaped adhered cells with contracted morphology with unidirectional proliferation and poorly developed actin stress fibers (Figure 8a–c). This type of morphology is similar to that observed by Lim et al.[35] for hFOB cells cultured on hydrophobic glass substrates. Conversely, the DBD treated polymer demixed surfaces ($PMMA_{75}PS_{25DBD}$, $PMMA_{50}PS_{50DBD}$, and $PMMA_{25}PS_{75DBD}$) showed many adhered cells with well spread morphology and a complex network of actin stress fibers (Figure 8d–f). This response is similar to that observed by Lim et al.[35] for hFOB cells grown on hydrophilic plasma treated quartz. In this type of positive cellular response, the development of cytoskeleton and focal adhesion complexes occur simultaneously with both contributions to changes in cell morphology, affecting one another.[36−38] For the polymer demixed surfaces, the hFOB cytoskeleton is developed only on the DBD-treated surfaces, indicating that the plasma-induced surface chemistry makes a more important contribution to cell response than a change in topography.

4. DISCUSSION

Spin-coating of PMMA/PS demixed blends produces surfaces with differing topographies and wettabilities. DBD plasma treatment of these polymer blends has been used to change the surface chemistry (oxidative functionalization) of the thin films to ascertain differences in cellular response based on chemistry vs topography. Since the two polymers are immiscible, phase separation takes place leading to a relatively disordered surface morphology. Chloroform has a high vapor pressure (18.6 kPa) at room temperature.[39] The Hildebrand solubility parameters of PS, PMMA and chloroform are 9.1, 9.5, and 9.3, respectively. Generally, the solubility of the polymer increases when its solubility parameter is closer to that of the solvent. The surface tension of the two polymers are similar and differences may vary according the method of evaluation.[40,41] Hence predicting which polymer will segregate to the top at equilibrium is difficult. Ton-That et al. have shown that the changes of the PMMA pit size in blend films of PS/PMMA is the result of the incomplete dewetting of a PMMA solution from the underlying PS solution during spin coating.[19,42] Walheim et al. have hypothesized that the distinct differences in the thin film domain structure and surface topography depend on the substrate surface energy and the relative solubilities of the two polymers in the common solvent.[21] Tanaka et al. proposed that incomplete wetting of the surface by the lower surface energy component will force the higher surface energy component to protrude from the film surface.[17] Heriot and Jones.[16] and Jukes et al.[29] have shown vertical stratification of the two polymers ending in a lateral phase-separated thin film.

The study by Heriot and Jones has been the most conclusive as they were able to study phase separation in spin-coated films of PMMA and PS beyond just the analysis of the final films.[22] During the spin-coating process, as the solvent evaporates, the system transforms from a one-phase region polymer/polymer/solvent phase diagram to a two-phase region of polymer/solvent and polymer/solvent. Heriot and Jones[22] hypothesize that early in this spin coating process, phase separation of the films takes place and forms two layers at the substrate and air interface: a PS-rich and a PMMA-rich one as seen in Figure 9. Fluid flow followed by solvent evaporation causes these layers

DOI: 10.1021/acsami.5b08073
ACS Appl. Mater. Interfaces XXXX, XXX, XXX−XXX

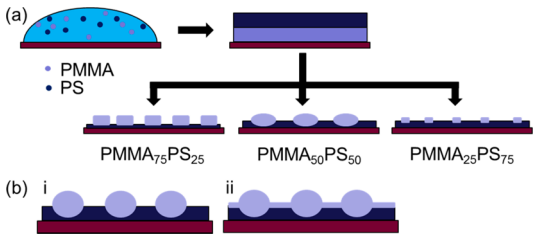

Figure 9. Schematic representation of (a) the spin-coating process and formation of final film morphology. (b) Structural models of PMMA/PS blends where the surface pits correspond to the pits in the interface or with lateral phase separation.

to thin.[43,44] As the films reach a critical threshold in thickness, instability at the interface between the two polymer layers develops due to a solvent-concentration gradient through the film.[22] The solvent at the surface evaporates much faster than in the bulk. The relative solubility of the two polymers in the solvent will play a factor in one of the phases being depleted of solvent quicker and will turn solid earlier than the other phase.[21] The instabilities increase to a point such that the highest interfacial protrusions will touch the top surfaces of the film; the film will break up rapidly into lateral domains. A secondary phase separation occurs simultaneously in the domains giving the final morphology of the films as seen in Figure 9a. Hence the morphology is a result of the interplay between the phase separation and dewetting during spin-coating.[22,43] Additionally, the phase separated morphology may not be at thermodynamic equilibrium, and achieving this equilibrium may be hampered by kinetic barriers associated with the nonequilibrium morphology.

In this study, the polymer demixed films were not at thermodynamic equilibrium with a PMMA rich phase segregating to the surface, even though its surface free energy is slightly higher than that of PS. This may be due to a lateral phase separation of the two polymers (Figure 9bi) or the formation of a continuous surface overlayer of PMMA (Figure 9bii). Given that the ToF-SIMS (depth of resolution of 2 nm and a lateral resolution of 100 μm^2) has contribution from PMMA and PS, it is more likely that the first scenario exists where lateral phase separation has occurred (Figure 9bi).

The DBD process results in the generation of reactive species which are transferred to the polymer surface through a flux of neutral particles, electrons, ions, and radicals, as well as from exposure to UV radiation. The energetic species generated in the plasma are produced in discrete pulses, with durations in the tens of nanoseconds time scale. This so-called "cold" plasma condition keeps surface damage by thermal effects to a minimum. Our group has previously shown with XPS and ToF-SIMS analysis, DBD treatment results in mainly surface oxidation of polymers with little or no oxygen inherent in its chemical structure such as PS and that polymers with oxygen such as PMMA undergo a combination of etching and oxidation.[25,45,46] Therefore, for the relatively short residence times in the DBD plasma as in this study, the PS surface roughness is only mildly etched, as determined by AFM. This indicates that the changes in wettability seen for PS is mainly a consequence of induced changes in surface chemistry.[25,46] For PMMA, the DBD processing can increase surface roughness slightly because of chain scission reactions that occurred in the surface region. Hence, in this case the change in wettability induced by DBD treatment can be a combination of oxidative surface chemistry and moderate surface roughening.[25,46] With the PMMA:PS polymer system studied here as PMMA segregates to the air interface, etching and oxidation of the surface is observed post DBD treatment.

Identifying which component polymer segregates to the air interface is important when assessing cell behavior, as cells only interact with the topmost layer of the substratum. In this case, we believe that the tops of the nanoislands are composed of PMMA and the pits are PS. Control experiments show that hFOBs do not adhere to pristine flat PMMA and PS, whereas the number of viable cells is significantly higher on the DBD treated pure polymer surfaces (Figures S2 and S3). This is in corroboration with previous work in our group that has demonstrated that short-term lens epithelial cell response on flat pure PMMA and PS surfaces is poor compared with the surfaces post DBD plasma treatment.[25] In this previous study, however, DBD plasma treatment increases the roughness and changes the surface chemistry of the PMMA and PS.[25] Therefore, it is not possible to determine the effect of each variable plays in increasing cellular response. In the present study, the nanotextured surfaces of PMMA:PS (regardless of what the topmost layer is) did not positively affect short-term hFOB response in comparison with flat samples. In comparison, post DBD plasma treatment, the change in surface chemistry that incorporates more polar groups has a dramatic effect on hFOB response. A salient point here is that even though the DBD plasma results in etching of nanotopographies, the feature heights have remained below 70 nm, which has been previously shown to be the threshold for nanoislands increasing cell response and above which disruption to integrin clustering and cell adhesion occurs.[4,10,11] Therefore, the increased cellular response can be attributed to surface chemistry in this polymer system and for this cell line.

Several reports in the literature demonstrate that isotropic nanotopgraphies of randomly distributed islands are capable of inducing differential osteoblastic response; however, these studies have used different polymers in the fabrication of their demixed surfaces.[9−11,47] In our study, short-term cytocompatibility was positively correlated with surface wettability, similar to previous reports[3−10] showing greater cell adhesion and spreading on more hydrophilic surfaces and that that the nanotopographical features here were insufficient to increase hFOB response. These findings are in agreement with other reports in the literature that analyzed osteoblast response to nanotextured surfaces. One of the early studies in the field, by Hendrich et al. have shown higher hFOB proliferation on smooth titanium surfaces and lower proliferation on rougher CoCrMo surfaces.[48] Additionally, hFOB proliferation on stainless steel and CoCrMo surfaces were similar despite significantly deferring roughnesses. Donahue and co-workers have shown that actin stress fibers and vinculin plaques were poorly developed on flat PS samples compared to surfaces with nanoislands.[11] However, when using a more hydrophilic polybromostyrene flat sample, the hFOB cells displayed well-developed actin stress fibers and vinculin plaques similar to surfaces with 11 nm nanoislands.[11] As such roughness aspects are not solely important but also the physicochemical composition of underlying biomaterial surfaces is necessary for the interpretation of in vitro cytocompatibility and in vivo biocompatibility results. Indeed, Curran and co-workers have also shown using model surfaces with polar functional groups (−OH, −COOH) stimulated mesenchymal stem cell response in terms of adhesion, proliferation and differentiation.[49−51]

DOI: 10.1021/acsami.5b08073
ACS Appl. Mater. Interfaces XXXX, XXX, XXX−XXX

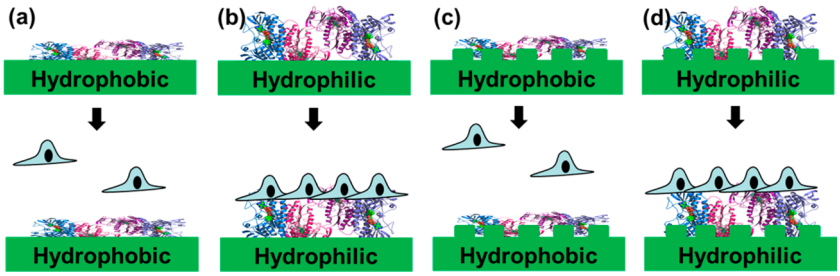

Figure 10. Schematic representation of the initial stages of cell adhesion on (a) flat hydrophobic, (b) flat hydrophilic, (c) nanotextured hydrophobic, and (d) nanotextured hydrophilic surfaces.

Cell adhesion is a multifaceted phenomenon with different factors having importance at the various stages of the process timeline.[44] For instance, surface chemistry, colloid forces and surface thermodynamics are known to be important early events in the cell adhesion process.[44] On the basis of our results, a schematic representation of the general mechanism involved in the initial stages of cell response to surface chemistry vs topography is given in Figure 10. On a flat hydrophobic surface, proteins flatten, denature and irreversibly adhere to the surface, thereby hindering protein turnover and reducing cellular adhesion and proliferation as seen in Figure 10a.[25] As most polymeric biomaterials are hydrophobic, plasma treatment is commonly carried out to oxidatively functionalize the surface which increases its hydrophilicity/wettability. The hydrophilic surface condition that occurs after plasma treatment will allow for protein turnover such that cell adhesion proteins adsorb to the surface leading to enhanced cell adhesion (Figure 10b).[25]

The introduction of nanoscale topographical features may affect the adsorption of cell adhesion proteins which can also directly affect cellular response.[49] However, the results from our study clearly show that the underlying physiochemical properties of the substrate are important and that variation in nanotopography does not increase hFOB cellular adhesion for this polymer demixed system as illustrated in Figure 10c. For the PMMA/PS demixed system and hFOB cell line, an increase in surface hydrophilicity/wettability induced by exposure to a DBD plasma results in a pronounced increase in cellular response (Figure 10d). We have previously shown that mesenchymal stem cells do respond to polymer demixed polycaprolactone (PCL)/PMMA mixtures without the need to alter their surface chemistry. This indicates that the role of surface chemistry vs topography effects in directing cell adhesion and proliferation are dependent on individual cell lines and physicochemical properties of the substratum.[15] These observations indicate that, when assessing cell response, the role played by the various contributing biomaterial characteristics should be evaluated both independently and communally.

5. CONCLUSIONS

In summary, PMMA/PS demixed thin films produced randomly distributed nanotopographies that ranged from nanoislands to nanopits. As the concentration of PMMA increased in the blend, a nanoisland topography becomes dominant, whereas when PS was in excess a nanopit topography dominated. PMMA tended to segregate to the top of the nanoislands and PS preferred the substrate interface. DBD treatment of the demixed films was carried out to assess the effects of surface chemistry vs topography effect on hFOB response. The nanotextured thin films did not elicit a proactive cellular response on their own; however, an increase in hydrophilicity via DBD treatment had a dramatic effect on cell adhesion for hFOBs. These results highlight the necessity of taking into consideration not only topographical contributions, but also the physicochemical composition of biomaterial surfaces for determining the mechanism of cellular adhesion and proliferation.

■ ASSOCIATED CONTENT

Supporting Information

The Supporting Information is available free of charge on the ACS Publications website at DOI: 10.1021/acsami.5b08073.

Tables S1 and S2 and Figures S1−S4 (PDF)

■ AUTHOR INFORMATION

Corresponding Author

*E-mail: r.dsa@liverpool.ac.uk.

Funding

Financial support from the Department for Employment and Learning, Northern Ireland under the Cross Border Research and Development Funding Programme−Strengthening the All-island Research Base for Functional Biomaterials (DEL-UU-05) is acknowledged.

Notes

The authors declare no competing financial interest.

■ REFERENCES

(1) Anselme, K.; Ploux, L.; Ponche, A. Cell/Material Interfaces: Influence of Surface Chemistry and Surface Topography on Cell Adhesion. *J. Adhes. Sci. Technol.* **2010**, *24*, 831−852.

(2) Lord, M. S.; Foss, M.; Besenbacher, F. Influence of Nanoscale Surface Topography on Protein Adsorption and Cellular Response. *Nano Today* **2010**, *5*, 66−78.

(3) Lamers, E.; van Horssen, R.; te Riet, J.; van Delft, F.C.M.J.M.; Luttge, R.; Walboomers, X. F.; Jansen, J. A. The Influence of Nanoscale Topographical Cues on Initial Osteoblast Morphology and M. *Eur. Cells Mater.* **2010**, *20*, 329−343.

(4) Biggs, M. J. P.; Richards, R. G.; Dalby, M. J. Nanotopographical Modification: A Regulator of Cellular Function Through Focal Adhesions. *Nanomedicine* **2010**, *6*, 619−633.

(5) Kunzler, T. P.; Huwiler, C.; Drobek, T.; Vörös, J.; Spencer, N. D. Systematic Study of Osteoblast Response to Nanotopography by Means of Nanoparticle-Density Gradients. *Biomaterials* **2007**, *28*, 5000−5006.

(6) Anselme, K.; Bigerelle, M. Role of Materials Surface Topography on Mammalian Cell Response. *Int. Mater. Rev.* **2011**, *56*, 243−266.

(7) Yim, E. K. F.; Reano, R. M.; Pang, S. W.; Yee, A. F.; Chen, C. S.; Leong, K. W. Nanopattern-Induced Changes in Morphology and Motility of Smooth Muscle Cells. *Biomaterials* **2005**, *26*, 5405−5413.

DOI: 10.1021/acsami.5b08073
ACS Appl. Mater. Interfaces XXXX, XXX, XXX−XXX

(8) Affrossman, S.; Henn, G.; O'Neill, S. A.; Pethrick, R. A.; Stamm, M. Surface Topography and Composition of Deuterated Polystyrene-Poly (bromostyrene) Blends. *Macromolecules* **1996**, *29*, 5010−5016.
(9) Lim, J. Y.; Donahue, H. J. Cell Sensing and Response to Micro- and Nanostructured Surfaces Produced by Chemical and Topographic Patterning. *Tissue Eng.* **2007**, *13*, 1879−1891.
(10) Lim, J. Y.; Hansen, J. C.; Siedlecki, C. A.; Hengstebeck, R. W.; Cheng, J.; Winograd, N.; Donahue, H. J. Osteoblast Adhesion on Poly(l-lactic Acid)/Polystyrene Demixed Thin Film Blends: Effect of Nanotopography, Surface Chemistry, and Wettability. *Biomacromolecules* **2005**, *6*, 3319−3327.
(11) Lim, J. Y.; Hansen, J. C.; Siedlecki, C. A.; Runt, J.; Donahue, H. J. Human Foetal Osteoblastic Cell Response to Polymer-Demixed Nanotopographic Interfaces. *J. R. Soc., Interface* **2005**, *2*, 97−108.
(12) Biggs, M. J. P.; Richards, R. G.; Dalby, M. J. Nanotopographical Modification: A Regulator of Cellular Function through Focal A dhesions. *Nanomedicine* **2010**, *6*, 619−633.
(13) Dalby, M.; Giannaras, D.; Riehle, M.; Gadegaard, N.; Affrossman, S.; Curtis, A. Rapid Fibroblast Adhesion to 27nm High Polymer Demixed Nano-Topography. *Biomaterials* **2004**, *25*, 77−83.
(14) Dalby, M.; Riehle, M.; Johnstone, H.; Affrossman, S.; Curtis, A. In Vitro Reaction of Endothelial Cells to Polymer Demixed Nanotopography. *Biomaterials* **2002**, *23*, 2945−2954.
(15) Khattak, M.; Pu, F.; Curran, J. M.; Hunt, J. A.; D'Sa, R. A. Human Mesenchymal Stem Cell Response to Poly(ε-caprolactone/Poly(methyl methacrylate) Demixed Thin Films. *J. Mater. Sci.: Mater. Med.* **2015**, *26*, 1−7.
(16) Dalby, M. J.; Riehle, M. O.; Johnstone, H.; Affrossman, S.; Curtis, A. S. G. In Vitro Reaction of Endothelial Cells to Polymer Demixed Nanotopography. *Biomaterials* **2002**, *23*, 2945−2954.
(17) Tanaka, K.; Takahara, A.; Kajiyama, T. Film Thickness Dependence of the Surface Structure of Immiscible Polystyrene/Poly(methyl methacrylate) Blends. *Macromolecules* **1996**, *29*, 3232−3239.
(18) Tanaka, K.; Takahara, A.; Kajiyama, T. Surface Molecular Aggregation Structure and Surface Molecular Motions of High-Molecular-Weight Polystyrene/Low-Molecular-Weight Poly(methyl methacrylate) Blend Films. *Macromolecules* **1998**, *31*, 863−869.
(19) Ton-That, C.; Shard, A.; Teare, D.; Bradley, R. XPS and AFM Surface Studies of Solvent-Cast PS/PMMA Blends. *Polymer* **2001**, *42*, 1121−1129.
(20) Ton-That, C.; Shard, A. G.; Bradley, R. H. Surface Feature Size of Spin Cast PS/PMMA Blends. *Polymer* **2002**, *43*, 4973−4977.
(21) Walheim, S.; Böltau, M.; Mlynek, J.; Krausch, G.; Steiner, U. Structure Formation via Polymer Demixing in Spin-Cast Films. *Macromolecules* **1997**, *30*, 4995−5003.
(22) Heriot, S. Y.; Jones, R. A. L. An Interfacial Instability in a Transient Wetting Layer Leads to Lateral Phase Separation in Thin Spin-Cast Polymer-Blend Films. *Nat. Mater.* **2005**, *4*, 782−786.
(23) Dekeyser, C.; Biltresse, S.; Marchand-Brynaert, J.; Rouxhet, P.; Dupont-Gillain, C. C. Submicrometer-Scale Heterogeneous Surfaces by PS−PMMA demixing. *Polymer* **2004**, *45*, 2211−2219.
(24) Ahn, D. U.; Wang, Z.; Campbell, I. P.; Stoykovich, M. P.; Ding, Y. Morphological Evolution of Thin PS/PMMA Films: Effects of Surface Energy and Blend Composition. *Polymer* **2012**, *53*, 4187−4194.
(25) D'Sa, R. A.; Burke, G. A.; Meenan, B. J. Protein Adhesion and Cell Response on Atmospheric Pressure Dielectric Barrier Discharge-Modified Polymer Surfaces. *Acta Biomater.* **2010**, *6*, 2609−2620.
(26) D'Sa, R. A.; Burke, G. A.; Meenan, B. J. Lens Epithelial Cell Response to Atmospheric Pressure Plasma Modified Poly-(methylmethacrylate) Surfaces. *J. Mater. Sci.: Mater. Med.* **2010**, *21*, 1703−1712.
(27) D'Sa, R. A.; Dickinson, P. J.; Raj, J.; Pierscionek, B. K.; Meenan, B. J. Inhibition of Lens Epithelial Cell Growth via Immobilisation of Hyaluronic Acid on Atmospheric Pressure Plasma Modified Polystyrene. *Soft Matter* **2011**, *7*, 608−617.
(28) D'Sa, R. A.; Raj, J.; McMahon, M.; McDowell, D. A.; Burke, G. A.; Meenan, B. J. Atmospheric Pressure Plasma Induced Grafting of Poly(ethylene glycol) onto Silicone Elastomers for Controlling Biological Response. *J. Colloid Interface Sci.* **2012**, *375*, 193−202.
(29) D'Sa, R. A.; Meenan, B. J. Chemical Grafting of Poly (ethylene glycol) methyl ether methacrylate onto Polymer Surfaces by Atmospheric Pressure Plasma Processing. *Langmuir* **2010**, *26*, 1894−1903.
(30) Gengenbach, T. R.; Vasic, Z. R.; Chatelier, R. C.; Griesser, H. J. A Multi-Technique Study of the Spontaneous Oxidation of N-Hexane Plasma Polymers. *J. Polym. Sci., Part A: Polym. Chem.* **1994**, *32*, 1399−1414.
(31) Kingshott, P.; Thissen, H.; Griesser, H. J. Effects of Cloud-Point Grafting, Chain Length, and Density of PEG Layers on Competitive Adsorption of Ocular Proteins. *Biomaterials* **2002**, *23*, 2043−2056.
(32) Al-Omari, W. M.; Mitchell, C. A.; Cunningham, J. L. Surface Roughness and Wettability of Enamel and Dentine Surfaces Prepared with Different Dental Burs. *J. Oral Rehabil.* **2001**, *28*, 645−650.
(33) Bico, J.; Tordeux, C.; Quéré, D. Rough Wetting. *Europhys. Lett.* **2001**, *55*, 214.
(34) Ton-That, C.; Shard, A. G.; Daley, R.; Bradley, R. H. Effects of Annealing on the Surface Composition and Morphology of PS/PMMA Blend. *Macromolecules* **2000**, *33*, 8453−8459.
(35) Lim, J. Y.; Taylor, A. F.; Li, Z.; Vogler, E. A.; Donahue, H. J. Integrin Expression and Osteopontin Regulation in Human Fetal Osteoblastic Cells Mediated by Substratum Surface Characteristics. *Tissue Eng.* **2005**, *11*, 19−29.
(36) Chen, C. S.; Alonso, J. L.; Ostuni, E.; Whitesides, G. M.; Ingber, D. E. Cell Shape provides Global Control of Focal Adhesion A ssembly. *Biochem. Biophys. Res. Commun.* **2003**, *307*, 355−361.
(37) Ezzell, R. M.; Goldmann, W. H.; Wang, N.; Parasharama, N.; Ingber, D. E. Vinculin Promotes Cell Spreading by Mechanically Coupling Integrins to the Cytoskeleton. *Exp. Cell Res.* **1997**, *231*, 14−26.
(38) Oakley, C.; Brunette, D. M. Topographic Compensation: Guidance and Directed Locomotion of Fibroblasts on Grooved Micromachined Substrata in the Absence of Microtubules. *Cell Motil. Cytoskeleton* **1995**, *31*, 45−58.
(39) Lide, D. R.: *CRC Handbook of Chemistry and Physics*; CRC Press: Boca Raton, 2004.
(40) Makoto, M.; Heng-Yong, N.; Wataru, M.; Hiroshi, T. Local Properties of Phase-Separated Polymer Surfaces by Force Microscopy. *Jpn. J. Appl. Phys.* **1994**, *33*, 3775.
(41) Wu, S. *Polymer Interface and Adhesion*. Marcel Dekker: New York, 1982; Chapter 5.
(42) Ton-That, C.; Shard, A.; Bradley, R. Surface Feature Size of Spin Cast PS/PMMA blends. *Polymer* **2002**, *43*, 4973−4977.
(43) Jukes, P. C.; Heriot, S. Y.; Sharp, J. S.; Jones, R. A. L. Time-Resolved Light Scattering Studies of Phase Separation in Thin Film Semiconducting Polymer Blends during Spin-Coating. *Macromolecules* **2005**, *38*, 2030−2032.
(44) Emslie, A. G.; Bonner, F. T.; Peck, L. G. Flow of a Viscous Liquid on a Rotating Disk. *J. Appl. Phys.* **1958**, *29*, 858−862.
(45) Borcia, G.; Anderson, C. A.; Brown, N. M. D. The Surface Oxidation of Selected Polymers using an Atmospheric Pressure Air Dielectric Barrier Discharge. Part II. *Appl. Surf. Sci.* **2004**, *225*, 186−197.
(46) D'Sa, R. A. *Surface Modification of Medically Relevant Polymers using Atmospheric Pressure Plasma Processing*; University of Ulster: Ulster, U.K., 2008.
(47) Liu, X.; Lim, J. Y.; Donahue, H. J.; Dhurjati, R.; Mastro, A. M.; Vogler, E. A. Influence of Substratum Surface Chemistry/Energy and Topography on the Human Fetal Osteoblastic Cell Line hFOB 1.19: Phenotypic and Genotypic Responses Observed In Vitro. *Biomaterials* **2007**, *28*, 4535−4550.
(48) Hendrich, C.; Nöth, U.; Stahl, U.; Merklein, F.; Rader, C. P.; Schütze, N.; Thull, R.; Tuan, R. S.; Eulert, J. Testing of Skeletal Implant Surfaces with Human Fetal Osteoblasts. *Clin. Orthop. Relat. Res.* **2002**, *394*, 278−289.
(49) Curran, J. M.; Chen, R.; Hunt, J. A. The Guidance of Human Mesenchymal Stem Cell Differentiation In Vitro by Controlled

DOI: 10.1021/acsami.5b08073
ACS Appl. Mater. Interfaces XXXX, XXX, XXX−XXX

Modifications to the Cell Substrate. *Biomaterials* **2006**, *27*, 4783−4793.
(50) Curran, J. M.; Chen, R.; Hunt, J. A. Controlling the Phenotype and Function of Mesenchymal Stem Cells In Vitro by Adhesion to Silane-Modified Clean Glass Surfaces. *Biomaterials* **2005**, *26*, 7057−7067.
(51) Curran, J. M.; Stokes, R.; Irvine, E.; Graham, D.; Amro, N.; Sanedrin, R.; Jamil, H.; Hunt, J. A. Introducing Dip Pen Nanolithography as a Tool for Controlling Stem Cell Behaviour: Unlocking the Potential of the Next Generation of Smart Materials in Regenerative Medicine. *Lab Chip* **2010**, *10*, 1662−1670.

DOI: 10.1021/acsami.5b08073
ACS Appl. Mater. Interfaces XXXX, XXX, XXX−XXX